RSC Advances

ROYAL SOCIETY OF CHEMISTRY

www.rsc.org/advances

A general and green approach to synthesize monodisperse ceria hollow spheres with enhanced photocatalytic activity

Weijun Deng[a], Donghui Chen[a,b], Jing Hu[b,*], Liang Chen[a,*]

[a]*College of Environmental Science and Engineering, Donghua University, Shanghai, 201620, China*
[b]*School of Perfume and Aroma Technology, Shanghai Institute of Technology, Shanghai 200235, China*

We report a general and green approach to synthesize monodisperse ceria hollow spheres with tunable shell structure. After ceria precursor is coated on monodisperse poly(styrene-co-acrylic acid) spheres via sol-gel method, ceria hollow spheres are successfully fabricated by calcination. The as-obtained hollow spheres exhibit enhanced photocatalytic activity under visible light. Our present work could not only provide a useful direction on scale-up fabrication of other metallic oxides hollow spheres with tunable shell structure, but also open a new doorway to ceria based photocatalyst synthesis under aqueous phase.

Keywords: monodisperse; ceria hollow sphere; sol-gel; calcination; photocatalysis

1. Introduction

Cerium (Ce) is the most abundant element, among rare earth family, which includes fifteen lanthanides together with scandium and yttrium. Cerium oxide (CeO_2) is widely used as a technically important materials in application of three-way catalysts (TWCs), low-temperature water-gas shift (WGS)[1], solid oxide fuel cells (SOFCs)[2], catalysis[3], oxygen sensors[4], glass polishing materials[5], and ultraviolet absorbent[6], photocatalysts for reduce of dyestuff[7], benzene[8], etc. The unique catalysis activity of ceria is attributed to its oxygen vacancies and oxygen buffering capacity[9, 10]. On cerium ion, the energy of the *4f* and *5d* electronic states are similar and the potential energy barrier to electron density distribution between them is low[11]. This closely links to how easily the cerium ions change their redox state. With the change of ambient partial pressure of oxygen, ceria forms a non-stoichiometric oxide of the general composition CeO_{2-x} through releasing or taking oxygen without decomposing. Oxygen vacancies, defects, normally dominate the ceria electronic and chemical intrinsic properties[12]. Ceria in the fluorite structure exhibits a few defects depending on partial pressure of oxygen. The energetics for defect formation may be substantially reduced in nanocrystalline oxides leading to markedly increased levels of nonstoichiometry and electronic carrier generation. Therefore, nanostructured ceria has attracted much attention for the improvement in the redox properties, transport properties and surface to volume ratio compared to the bulk materials. In the last decades, various ceria nanostructures were synthesized with defined shapes such as nanowires[13], nanorods[14], nanotubes[15], nanocubes[16], nanosheets[17], nanosphere[18], and ordered macroporous framework[19] which largely enhanced ceria performance in catalysis. Because the different sizes, structures, shapes of nanomaterial pose different properties and application, controlled sizes and morphologies are of critical importance to nanomaterial performance. Due to different absorptions and reactions, CeO_2 nanoshapes should be optimized for effective catalysis[20].

From morphology, hollow micro/nanospheres have attracted tremendous interests due to their well-defined shape, low density, large surface area, functional characteristics and a wide range of potential applications such as catalyst, lithium-ion batteries, biomedical applications, and gas sensors[21-23]. Titanium oxide spheres were photocatalytically more active and efficient than Degussa P25 for the photodecomposition of 2-chlorophenol[24]. A variety of chemical and physicochemical strategies with templates or without templates have been employed to prepare inorganic hollow spheres[22]. Ceria hollow spheres can also be fabricated with templates or without templates strategy. Template-free hydrothermal method has been employed to fabricate monodisperse CeO_2 hollow spheres with better catalytic properties of CO oxidation[25-27]. The Ostwald ripening process was proposed as larger crystals of outside grow from those inside with smaller size, which have higher solubility than the larger ones. Voids form and grow gradually in the cores of large aggregates. This process is time consuming and hollow spheres shape is difficult

*To whom correspondence should be addressed. Tel.: +862167792534.

to attain. Ostwald ripening needs further studies in support of fabrication mechanism. Template strategy is more promising for reproducibility. Template assisted method is the most common to fabricate inorganic hollow spheres. Many compounds such as silica, carbon, biomaterials, polymeric particles, can be chosen as templates to fabricate ceria hollow spheres. The final hollow sphere shapes and sizes are essentially dependent on that of templates. Ceria microporous hollow spheres with 12 nm thin layers of shell were templated by colloidal silica of 200 nm[28, 29]. By using lotus flower pollen[30] and rape pollen[31] as template, ceria hollow microspheres with improved photocatalytic activity were obtained. Carbon spheres were also successfully used as model for porous ceria hollow microspheres fabrication[30]. Nonetheless, their inherent demerits are obvious. Etching silica core with high concentration of caustic soda or HF is essential to obtain hollow spheres structures. Bio-templates such as flower pollen, rape pollen, are limited in resource for industrial production. Carbon spheres are effective templates, however, the fabrication process are complicated, tedious and hollow spheres tend to collapse under extremely high temperature for carbon particles removal. Templating against polystyrene (PS) is a common approach to fabricate TiO_2, SiO_2, SnO_2 hollow spheres[22]. However, there is no report adopting pure PS to prepare ceria hollow spheres. By templating against PS beads cross-linked with divinyl benzene, Shchukin and Caruso prepared titania, zirconia, tin oxide, and ceria hollow spheres[24]. The hydroxyl functionalized PS beads with a diameter of 11.5 um were dried, and then soaked in sol of cerium oxide. By successful infiltration and templating, monodisperse, nonaggregated spheres with a porous surface and inner structure were obtained. Nonetheless, there are two problems that have not yet been addressed: (i) the process tends to be complicate and time consuming. It is of great interest to develop a simple and green approach in aqueous phase which is suitable for scale up production. (ii) there is no description on photocatalytical properties of the as-obtained ceria hollow spheres. It is also of great interest to investigate the photocatalytic activity of ceria hollow spheres.

In this study, a general and green approach to fabricate monodisperse ceria hollow spheres with enhanced photocatalytic activity, is described. In comparison with other techniques, the primary differences and advantages of this approach are: a) there is no specific surface modification on template, no specific solvent and no complex reaction during the process; b) our present work not only provides a useful direction on scale-up fabrication of other metallic oxides hollow spheres with tunable shell structure, but also opens a new doorway to ceria based photocatalyst synthesis under aqueous phase. The as-obtained ceria hollow spheres exhibit enhanced photocatalytic activity under visible light.

2. Experimental

Materials

Styrene (S, ≥99%), acrylic acid (AA, ≥98%), ammonium persulfate (APS, ≥98%), cerium nitrate hexahydrate ($Ce(NO_3)_3.6H_2O$, ≥99%), absolute ethanol (EtOH, ≥99.7 %), concentrated ammonia solution (25 wt% NH_3 in water), sodium hydroxide (NaOH, 96%) were purchased from Sinopharm Chemical Reagent Corp. CeO_2 nanoparticles 30 nm in diameter were purchased from Jingrui Materials Company. All chemicals were used as received without further purification. Millipore water was used in all experiments.

Synthesis of ceria hollow spheres

Monodisperse ceria hollow spheres were fabricated with polymer sphere-template sol-gel strategy. Colloidal PSAA spheres were first synthesized using soap-free emulsion polymerization[32]. In a typical experiment, styrene (9.0 g), acrylic acid (1.0 g) and H_2O (100 g) were mixed in a 250 mL three-neck flask and deoxygenated by bubbling nitrogen gas at room temperature for 30 min. The mixture was heated to 70 ^oC at a stirring rate of 200 rpm and potassium persulfate solution (0.1 g in 10 mL of H_2O) was injected. The polymerization continued further for 10 h. The PSAA colloidal spheres were centrifuged and redispersed into H_2O for further use. Then, PSAA colloidal suspension (2 g), H_2O (25 mL) and 20 mL cerium nitrate solution (0.434 g of cerium nitrate hexahydrate in 20 mL of H_2O) were added in order and stirred at 60 ^oC for 2 h. 20 mL ammonia solution (0.2 mL concentrated ammonia solution in 20 mL of water) was added dropwisely within 1 h and temperature was kept at 60 ^oC for 2 h. The suspension was naturally cooled down and left for 2 h. Afterwards, the suspension was centrifuged and dried and finally calcinated at 500 ^oC in air for 3 h. The detailed experimental conditions and results are summarized in Table 1.

Characterization

The morphology and structure of the as-prepared products were observed using scanning electron microscopy (SEM) and transmission electron microscopy (TEM). SEM images were obtained using a Philips XL 30 field emission microscope at an accelerating voltage of 10 kV. TEM images were taken on a Hitachi H-800 transmission electron microscope at 75 kV. Thermal gravimetric analysis (TGA) was carried out with a TAQ 5000 at a heating rate of 10 ^{o}C min^{-1} in nitrogen (gas flow=40 mL min^{-1}). Fourier transform infrared spectrometer (FTIR) spectrum was obtained with a Nicolet Nexus 470 FTIR using powder-pressed KBr pellets. Nitrogen adsorption and desorption experiments were performed at 77 K on a NOVA 4000 gas adsorption analyzer (Quantachrome Corp.). The crystallinity of the sample after calcination was investigated by XRD on a Japan Rigaku D/Max-γA rotating anode X-ray diffractometer at a scanning rate of 0.02^{o} s^{-1} in the 2θ range from 10 to 80^{o}.The surface area was determined using the Brunauer-Emmett-Teller (BET) method. The mesopore volume and pore size distribution were calculated from nitrogen desorption isotherm curves using the Brunauer-Joyner-Halenda (BJH) method.

Photocatalytic evaluation

The photocatalytic experiments were carried out using the degradation of RhB in an aqueous solution in a photochemical reactor (BL-GLH-V, Shanghai Bilang photocatalytic equipments Plant, China), equipped with a 300W Xe lamp combined with a 420nm cut-off filter as the light source, which was about 15 cm from the liquid surface of the suspensions. All photocatalytic reactions were performed using the same initial conditions: 50mL of 20 mg L^{-1} of RhB dye was mixed with 10 mg catalyst under constant magnetic stirring. Before irradiation, the suspension was stirred for 30 min in the dark to reach adsorption–desorption equilibrium. At given time intervals, the analytic samples exposed for different time intervals were taken out of the reaction suspension and centrifuged at 12,000 rpm for 2 min to remove CeO_2 particles. The concentration of RhB was determined by UV-vis spectroscopy (UV-1800, Shimadzu, Japan). For the sake of comparison, the photocatalytic properties of blank and commercial CeO_2 nanoparticles (30 nm in diameter) were monitored at equal conditions.

Table 1 The synthesis conditions and nanostructures ceria hollow spheres

Entry [a] no.	Cerium nitrate solution (mL)	Ammonia[b] (mL)	Temperature of sol-gel reaction (^{o}C)	Morphology
1	20	0	60	no hollow sphere
2	20	0.05	60	no hollow sphere
3	20	0.1	60	less hollow spheres produced, partial sphere morphology with thin shell
4	20	0.15	60	hollow spheres, partial spheres morphology
5	20	0.2	60	hollow spheres
6	20	0.25	60	hollow spheres
7	20	0.3	60	slightly aggregated hollow spheres
8	20	0.4	60	aggregated hollow spheres
9	20	0.5	60	heavily aggregated hollow spheres
10	20	0.6	60	heavily aggregated and distorted spheres morphology
11	10	0.2	60	no hollow sphere
12	12	0.2	60	less hollow spheres produced, partial sphere morphology with thin shell

13	14	0.2	60	hollow spheres, thin shell
14	16	0.2	60	hollow spheres
15	18	0.2	60	hollow spheres
16	22	0.2	60	hollow spheres
17	24	0.2	60	lightly aggregated hollow spheres
18	26	0.2	60	heavily aggregated hollow spheres
19	20	0.2	40	less hollow spheres produced
20	20	0.2	50	hollow spheres
21	20	0.2	70	aggregated hollow spheres
22	20	0.2	80	aggregated hollow spheres, rough shells

[a] For all entries, the amount of the polymer spheres was 0.1 g. [b]The entries, sol-gel reactions with NaOH and hexamethylenetetramine were not shown here but used and mentioned in paper.

3. Results and discussion

Synthesis of ceria hollow spheres

Briefly, colloidal PSAA spheres were first synthesized using soap-free emulsion polymerization, and then core-shell $Ce(OH)_3$@PSAA composite spheres were prepared based on PSAA spheres with sol-gel reaction. Finally the cores of PSAA were removed by calcination and shells of $Ce(OH)_3$ simultaneously changed to hollow spheres with crystalline structure.

Fig. 1a and b are SEM images of PSAA spheres and $Ce(OH)_3$@PSAA composite spheres. It is observed that the spheres are homogenous. The surface roughness of spheres in Fig.1b compared to that in Fig. 1a, confirms the formation of $Ce(OH)_3$ shells surrounding the PSAA core particles. In Fig. 1a, the diameter of spheres is approximately 200 nm and in Fig. 1b, the diameter of spheres is approximately 240 nm. The increase in diameter is attributed to $Ce(OH)_3$ particles formation in sol-gel reaction. In our method, the comonomer of acrylic acid is added to negatively charge PS spheres with $–COO^-$ groups. When ceria precursor is mixed with PSAA spheres, Ce^{3+} ions are rapidly captured on the surface of PSAA beads via electrostatic interaction. Ammonia controls the pH of sol-gel system by slowly release of –OH- ions, as shown in equation (1). $Ce(OH)_3$ particles quickly form when cerium ions combine –OH- ions, as in equation (2). The absorbed Ce^{3+} ions by $-COO^-$ on PSAA sphere surfaces serves as nucleation sites during sol-gel reaction. This is the ideal model for formation of $Ce(OH)_3$ shells surrounding the PSAA core particles.

$$NH_3 \bullet H_2O = NH_4^+ + OH^- \quad (1)$$

$$Ce^{3+} + 3OH^- = Ce(OH)_3 \quad (2)$$

The result of visional observation is in accordance with DLS analysis. Fig. 1c and d are DLS analysis of PSAA spheres and composite spheres, respectively. The average diameter of PSAA spheres is 197.54 nm and the average diameter of composite spheres is 238.56 nm. Both PSAA spheres and $Ce(OH)_3$@PSAA composite spheres are monodisperse. Therefore, the as-obtained ceria hollow sphere are monodisperse.

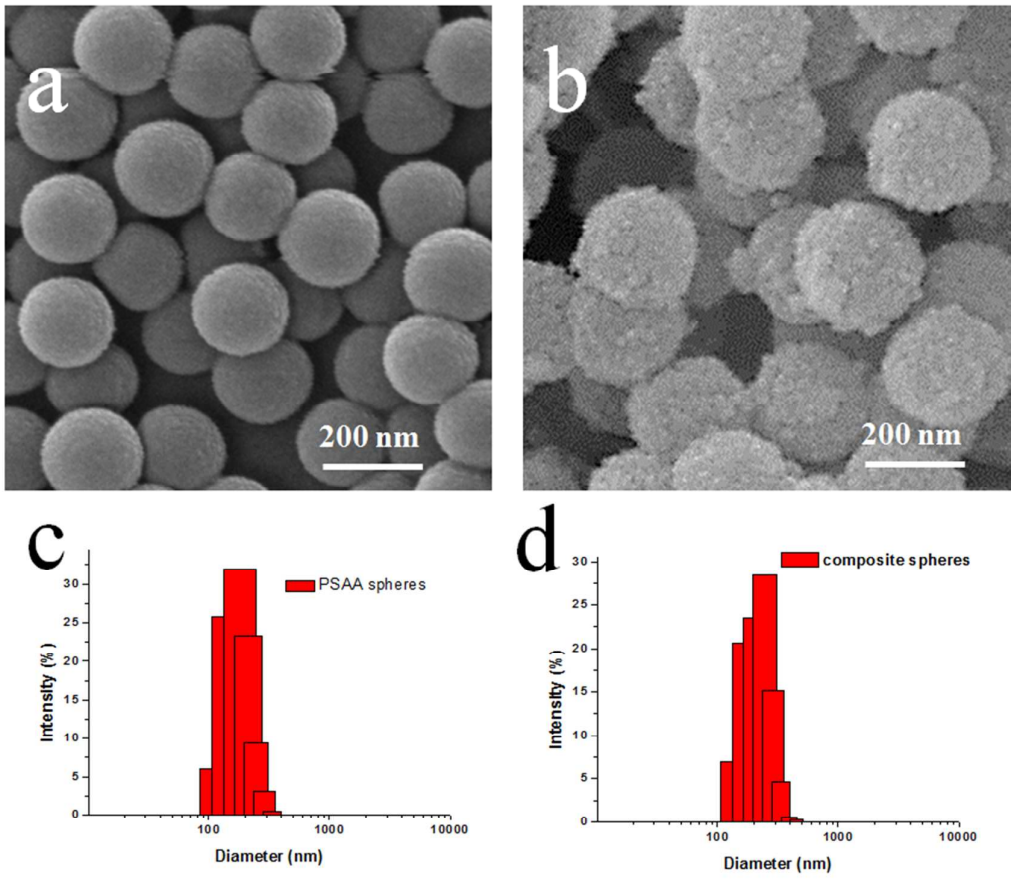

Fig. 1 SEM images of PSAA spheres (a) and Ce(OH)3@PSAA composite spheres (b) and DLS results of PSAA spheres (c) and Ce(OH)3@PSAA composite spheres (d)

Fig. 2a further illustrates the TGA and DSC curves of the composite spheres. The weight loss at temperature 30-270 ^{o}C is attributed to the release of combined water. The weight loss at temperature 270-370 ^{o}C is due to decomposition of PSAA template. At beginning, PSAA slowly decomposes at temperature 270-350 ^{o}C. At temperature of 350 ^{o}C, the mass loss is round 5%. The fast elevated temperature leads to PSAA rapid decomposition which produces gas and the resultant gas finally escapes outward. This indicates that organic templates release abruptly out of the constraint of inorganic shell. DSC result additionally indicates that at temperature of 350 ^{o}C the hybrid PSAA spheres release energy abruptly. The marked part in Fig. 4a is a hole on hollow sphere generated from such abrupt energy. The energy from this composite sphere is not strong enough like other spheres with holes, and a piece of shell remains linked to the hollow spheres. This is the reason for holes formation on ceria hollow spheres. The precise temperature control at this temperature is possible to reduce holes on hollow spheres. At temperature 370-600 ^{o}C, there is less mass loss. However, the shell of composite spheres is oxidized in the air to CeO_2 crystalline structure, as shown in equation (3), where $0<x<0.5$ and the majority of CeO_{2-x} in our synthesis is CeO_2. The color of sample changes from white to pale yellow.

$$4Ce(OH)_3(Amorphous)+(1-2x)O_2=4CeO_{2-x}(Crystallite)+6H_2O \quad (3)$$

Assuming that 1 g of PSAA and 0.434 g of cerium nitrate hexahydrate could be theoretically transformed into 1.434 g of composite spheres according to experimental recipe. TGA result shows the remaining mass is approximately 60 wt. % after 500 ^{o}C, which almost matches the theoretical calculation. It is indicated that the as-obtained ceria hollow spheres has no component of PSAA and that PSAA has entirely decomposed after calcination.

Moreover, the typical FTIR spectra of PSAA spheres, composite spheres and ceria hollow spheres after calcination at 500 ^{o}C for the sake of comparison are demonstrated in Fig. 2b. The peaks at 3062 cm^{-1}, 2961 cm^{-1}, 1602 cm^{-1} correspond to the vibration absorptions of –CH groups, $=CH_2$

groups, and to the vibration of C=C groups, respectively. The typical bands of PSAA appear in PSAA curve and composite curve, however, disappear in ceria hollow spheres curve. In FTIR spectra, it is well explained that PSAA spheres were completely removed by calcination.

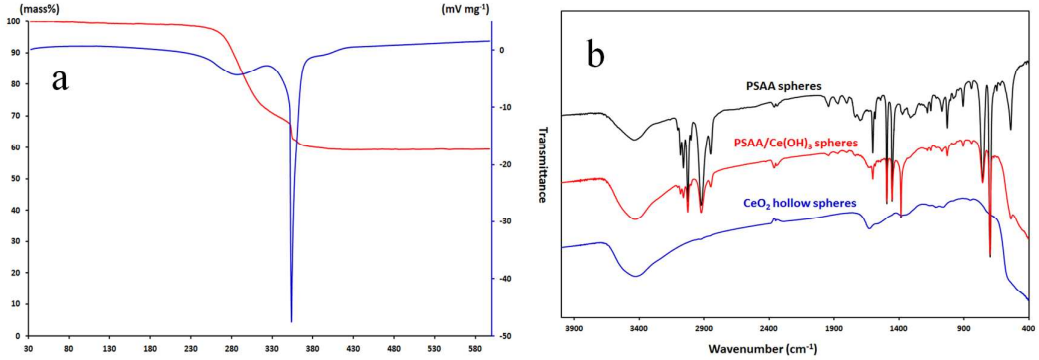

Fig.2 (a), TGA and DSC analysis of composite spheres. The red cure is TGA and blue cure is DSC curve. (b), FTIR results of PSAA spheres, composite spheres and ceria hollow spheres

To ensure that PSAA spheres were successfully modified in sol-gel reaction, EDX analysis are provided as useful evidence. Fig. 3 is the EDX result of composite spheres. There are four elements in composite spheres, i.e. C, O, N and Ce. The weight ratio of C is round 40%, indicating that the main part of composite spheres was organic. Weight ratio of Ce is 30-40%, verifying that the composite spheres contain cerium. Weight of O comes from both PSAA and $Ce(OH)_3$ shell. N comes from precursor $Ce(NO_3)_3$. Therefore, the composite spheres have organic polymer component, ceria component. According to the theoretical calculation based on the weight ration of Ce, the shell with CeO_2 crystalline structure have 38.3% on the weight of composite spheres, which agrees well with TGA analysis.

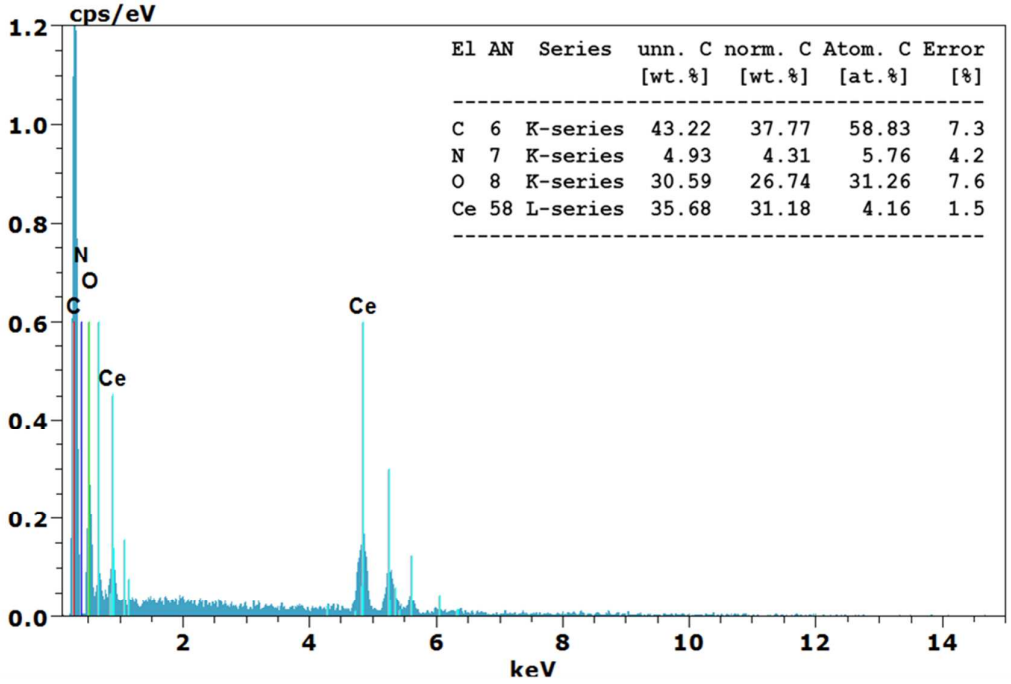

Fig. 3 EDX result of composite spheres with optimized conditions of entry no. 5

Morphology and structure of ceria hollow spheres

Fig. 4a and b present typical SEM and TEM images of product derived from our general and green approach. The as-obtained ceria hollow spheres are homogeneous and have an average diameter of 230 nm. In Fig. 4a, it is observed that the surface of spheres is rough, indicating that the size of particles sitting on surface is big. Comparison of TiO_2 hollow spheres with similar strategy indicates that the TiO_2 hollow spheres has smoother surface. This could be explained by the radius

of cerium ions is bigger than that of titanium ions. In Fig. 4a, there are holes on spheres which are dark and distinguished to their surroundings. This clearly shows that they are hollow inside. In Fig. 4b, the obvious contrast between the dark shell and the grey core confirms that these spheres have hollow structure. In Fig. 4b, it is also found that the hollow spheres are 230 nm in diameter and 17 nm in thickness of shells. Fig. 4c is HRTEM image of a typical ceria hollow sphere revealing that the shell of hollow sphere was 17 nm in thickness. Ceria hollow spheres are composed of numerous nanoparticles with a crystallite size about 5-7 nm. In addition, there are many voids (<5nm in width) among the small nanoparticles based on the color contrast of the image, revealing the mesoporous structure of the ceria hollow spheres. These voids not only provide efficient transport pathways to the interior, which is critical for catalyst, delivery, and other applications, but also allow multireflections of electromagnetic waves, such as ultraviolet and visible light, within their interior cavities, endowing these spheres with greatly enhanced properties. Fig. 4d clearly shows the lattice fringes, indicating high crystallinity of the shells. The lattice spacing has been determined as 0.31 nm, which correspond to the interplane distances of (111) of CeO_2. More oxygen vacancies were found on (111) and (310) surfaces than that in the bulk of crystal, indicating high catalytic activity on the shell[33].

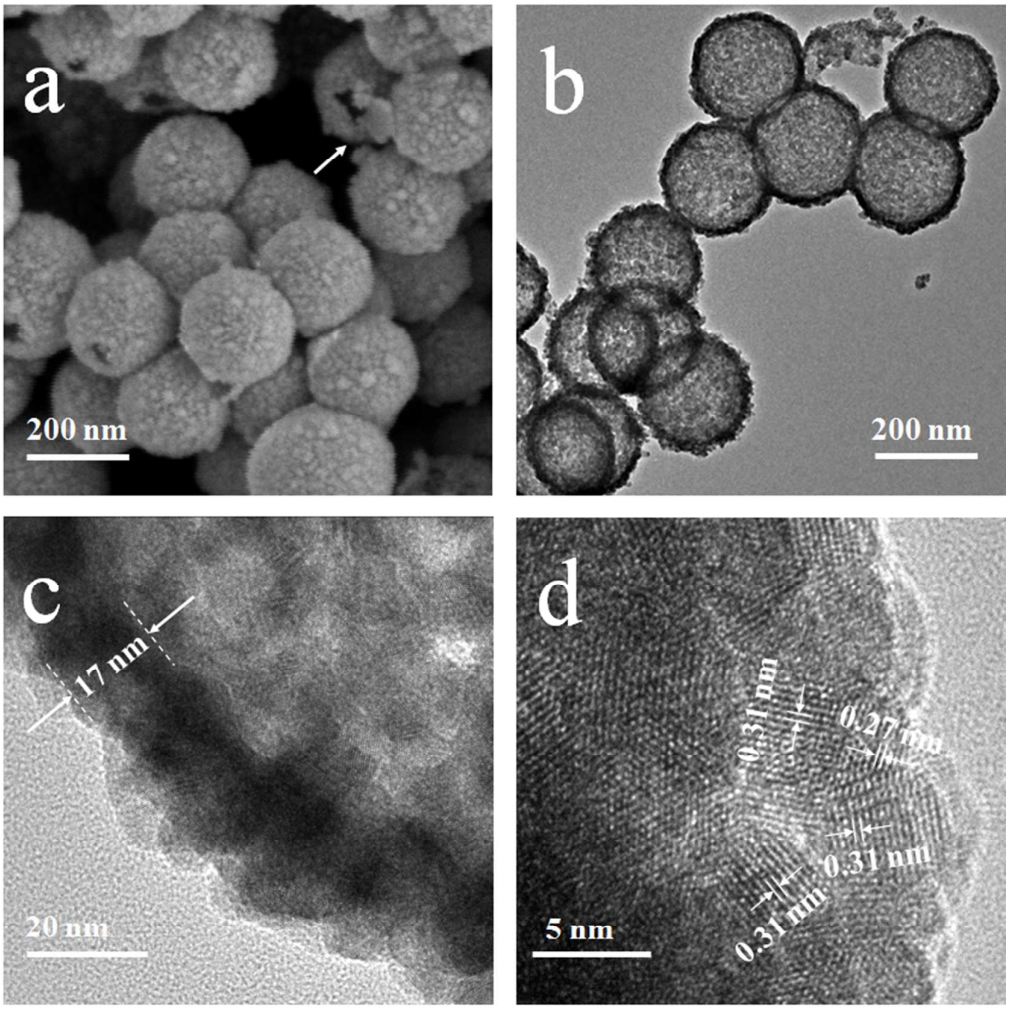

Fig.4 SEM (a), TEM (b) and HRTEM (c, d) images of ceria hollow spheres with optimized conditions of entry no. 5

XRD pattern of the as-obtained ceria hollow spheres is displayed in Fig. 5a. It can be seen clearly that they possess the crystallinity structure, which is in accordance with the selected area electron diffraction pattern (SAED) result in Fig 5b. The diffraction peaks at 2θ values of 28.6, 33.1, 47.5, 56.3, 59.1, 69.4, 76.7 and 79.1 are ascribed to the (111), (200), (220), (311), (222), (400), (331)

and (420) facets of cerianite CeO_2 (JCPDS No. 34–0394). Fig. 5b is SEAD pattern of a single ceria hollow sphere in Fig. 4c showing the typical polycrystalline structure of as obtained sample, which is in accordance with the XRD result. Thus, conclusion is drawn that as obtained hollow spheres were formed by many tiny grains in different orientations.

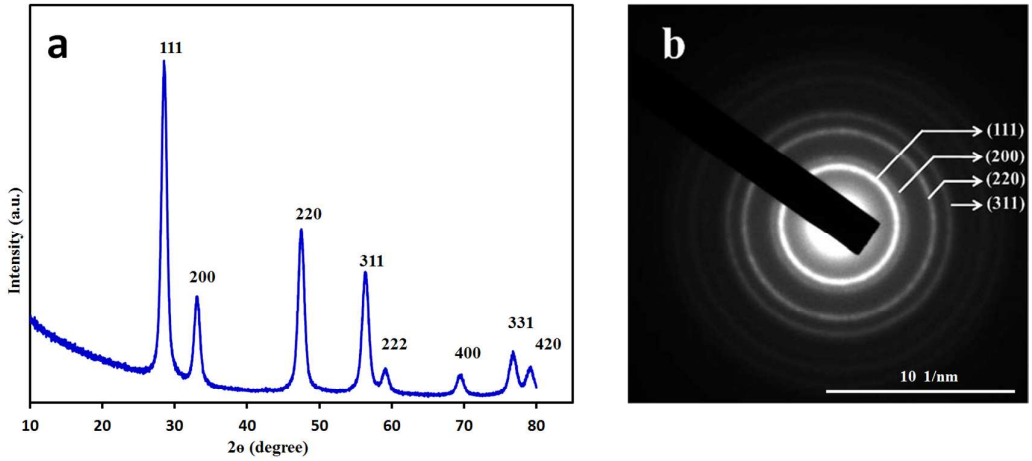

Fig 5. XRD and SAED images of ceria hollow spheres with optimized conditions of entry no. 5

Fig. 6a demonstrates the typical nitrogen adsorption/desorption isotherms of the as-obtained ceria hollow spheres. The nitrogen adsorption/desorption isotherms show typical type-IV curves, revealing the characteristics of mesoporous materials. No evident adsorption is observed in the isotherm of the as-obtained ceria hollow spheres, indicating the absence of any pores. The hollow spheres show a much larger surface area, 60.6 m^2 g^{-1}, pore volume (0.552 cm3 g^{-1}) and micropore surface area (65.5 m^2 g^{-1}). On the contrast, commercial ceria nanoparticles in size of 30 nm in diameter have only 12.95 m^2 g^{-1} of surface area.

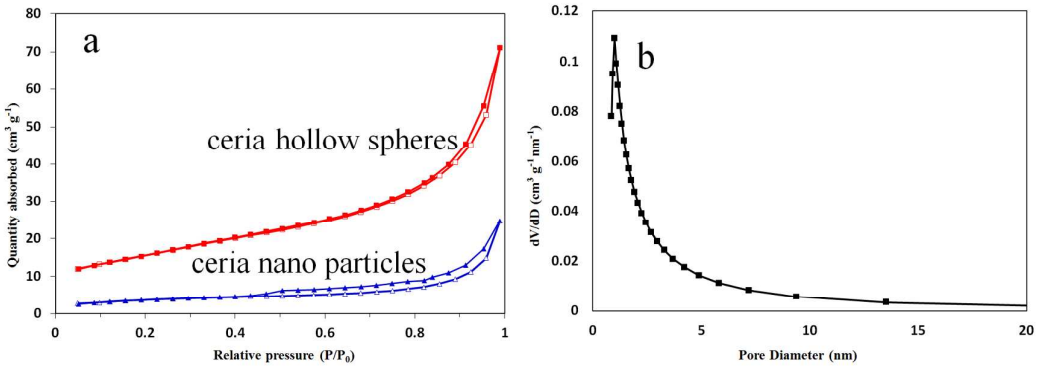

Fig. 6 Nitrogen adsorption/desorption isotherms (a) as-obtained ceria hollow spheres and commercial nanoparticles 30 nanometer in diameter and mesopore size distribution (b) of t as-obtained ceria hollow spheres

Effect of amount of ammonia

In coating process, ammonia was added to the PSAA suspension for the sol-gel reaction. To understand the function of ammonia in the formation process of ceria hollow spheres, control experiments without or with 0.05 mL ammonia were carried out as entry 1, 2. As result, no hollow spheres were produced with SEM observation, indicating that ceria was not coated on PSAA spheres. Fig. 7a-h displays the SEM images of the eight samples obtained from different amounts of ammonia, as shown entries no. 3-10, respectively. In Fig. 7a, at the ammonia amount of 0.1 mL, less ceria hollow spheres were produced. Most of them have partial hollow sphere morphology and the shell is very thin, indicating that PSAA was less coated by $Ce(OH)_3$. This shortage is improved in Fig 7b of entry 4. Hollow spheres morphology is most satisfying in Fig 7c-d, more intact and separated, although with partial cracks from calcination. In Fig 7e-h, aggregation of hollow spheres increases gradually. Meanwhile, it is found that more and more particles are sitting on the shells. Especially, in Fig 7f and g, the shell of hollow spheres are coarse.

The reason for this is the fast self-nucleation of $Ce(OH)_3$ nanoparticles due to more ammonia. To further understand the formation process of ceria hollow spheres, SEM of composite spheres were shown in Fig. 8a-d. In Fig 8a, the surface of spheres is smooth. In Fig 8b, c, the surface roughness of spheres compared to that of original PSAA particles confirms the formation of $Ce(OH)_3$ nanoparticles surrounding the PSAA core particles. In Fig 7h, there are not only heavy aggregation but also distorted sphere morphology. High amount ammonia has changed the shape of PSAA spheres. However, when amount of ammonia was increased to 0.6 mL the PSAA core began to dissolve and the core were incompletely dissolved in medium. To further verify this point, a control experiment was carried out, with 3 mL ammonia and without ceria precursor. As the result, all PSAA particles disappeared, indicating that the PSAA particles were completely dissolved in the medium, similarly as shown in literature[34]. The pioneer work from Wu and co-workers has described the correlation between morphology of silica hollow spheres and ammonia amount in the fabrication process[35]. Similarly, in our fabrication process, ammonia at high concentration contributed to faster dissolution rate of PSAA particles and faster precipitation rate of $Ce(OH)_3$. In Fig 7h, the obtained hollow spheres are seriously deformed which are attributed to faster dissolution rate of PSAA particles. The obtained hollow spheres are aggregated which are attributable to relative faster precipitation rate of $Ce(OH)_3$. The core of PSAA particles was unable to capture the rapidly forming $Ce(OH)_3$ particles and as result, they connected each other forming aggregation.

Interestingly, NaOH and hexamethylenetetramine other than ammonia were also used in coating process for sol-gel condition. In the former case, with even tiny amount of 0.05 g diluted in 20 mL water and gradual addition in 2h, no hollow spheres can be found with SEM observation. This is explained by the fast self-nucleation of $Ce(OH)_3$ nanoparticles caused by sharp pH increase. In the latter case, ceria hollow spheres can be generated until hexamethylenetetramine was increased to 20 g. Hexamethylenetetramine mildly generates OH- in sol-gel condition, however, it was consumed 5-7 times to the amount of cerium nitrate and it is not cheap in scale-up production. Therefore, the selection of ammonia is more suitable for scale-up fabrication of ceria hollow spheres.

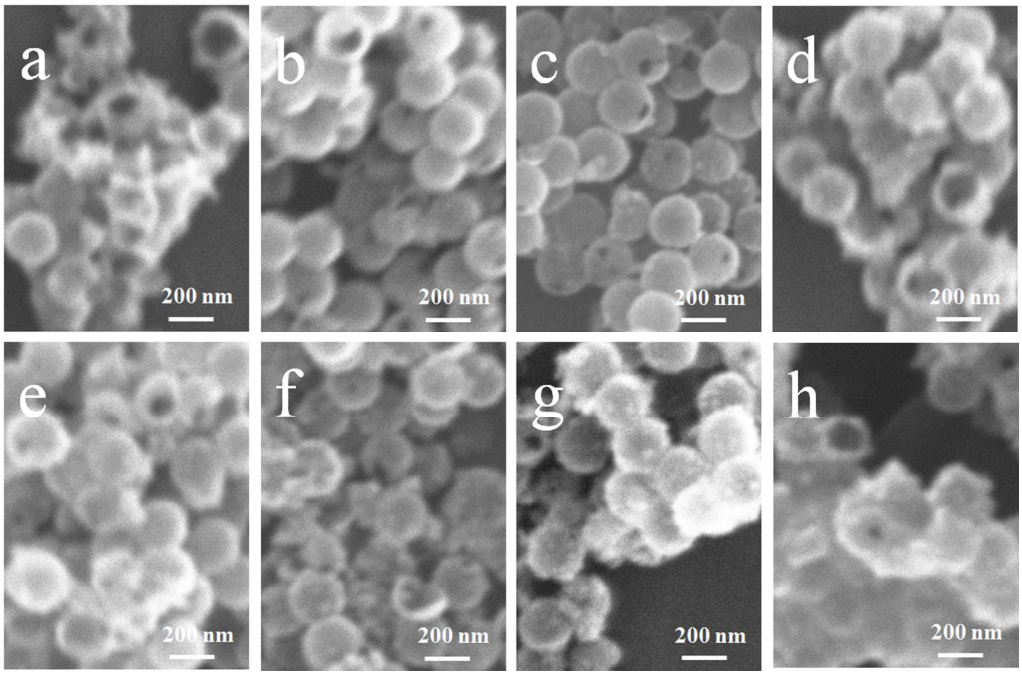

Fig. 7 SEM images of ceria hollow spheres with various amounts of ammonia from 0.1 mL to 0.6 mL

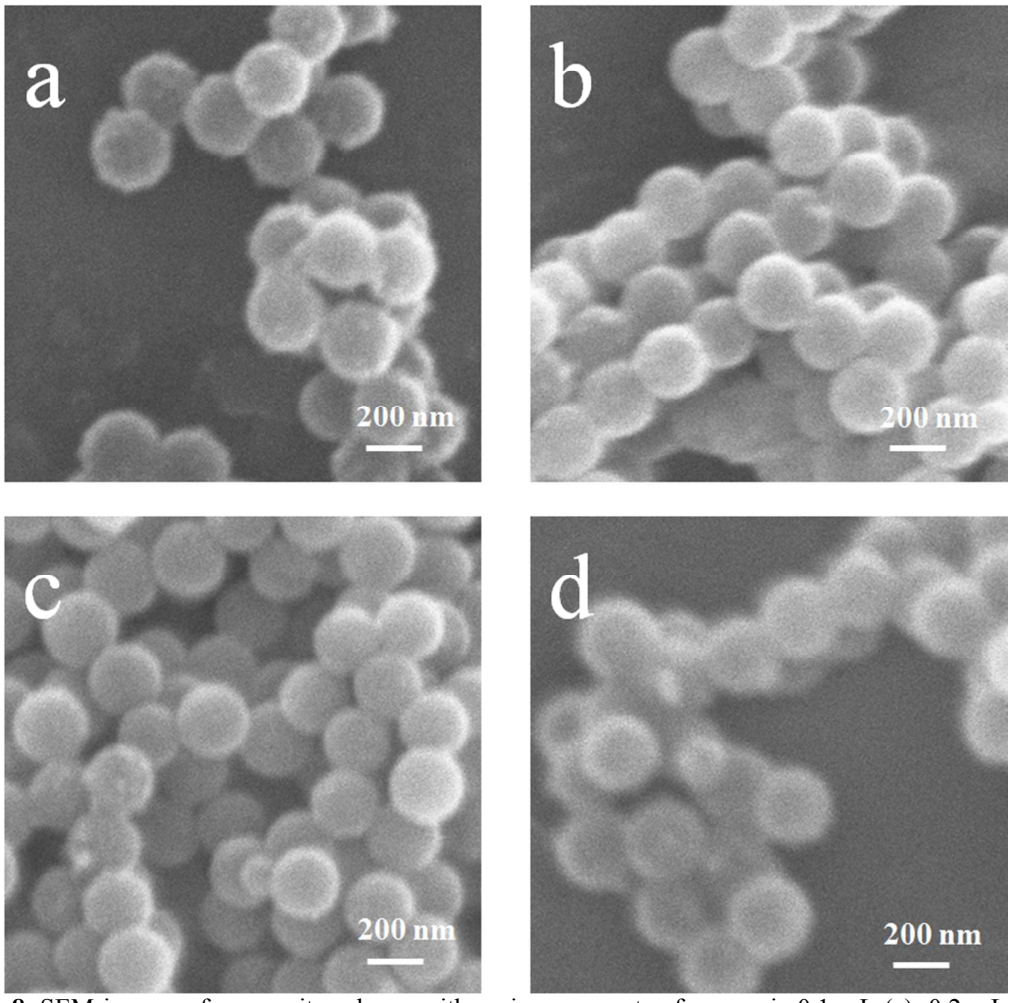

Fig 8. SEM images of composite spheres with various amounts of ammonia 0.1 mL (c), 0.2 mL (b), 0.25 mL (a) and 0.3 mL (d)

Effect of amount of precursor

Cerium nitrate concentration impacts on the surface deposition of composite spheres and thus impacts the thickness of ceria hollow spheres. When cerium nitrate was relatively low, e.g., 10, 12 mL in entries 11 and 12, PSAA colloid was coated by a small amount of $Ce(OH)_3$ nanoparticles. As results, the shells were too thin to maintain the hollow structure during calcination, and there were no hollow spheres or partially collapsed hollow spheres produced. Fig. 9 a-f are SEM images of entries 13-18, respectively. More cerium nitrate is used, more nanoparticles deposit onto surfaces of the PSAA colloid. From Fig. 8a-f, the shell of hollow spheres increases from 10 nm to 40 nm. Interestingly, the observation from Fig. 9a-b shows that there are more holes and cracks. The thicker shell is helpful to restrain the hollow spheres shapes. However, at higher cerium nitrate amount of 26 mL in Fig 9f, heavy aggregation of spheres is observed probably due to fast self-nucleation of $Ce(OH)_3$ nanoparticles in sol-gel system, suggesting that the PSAA core particles are unable to capture the rapidly forming $Ce(OH)_3$ particles and they connected each other forming aggregation. Thus, uniform shell thickness of the monodisperse ceria hollow spheres could easily be tailored by simply altering the concentration of cerium nitrate in the present study.

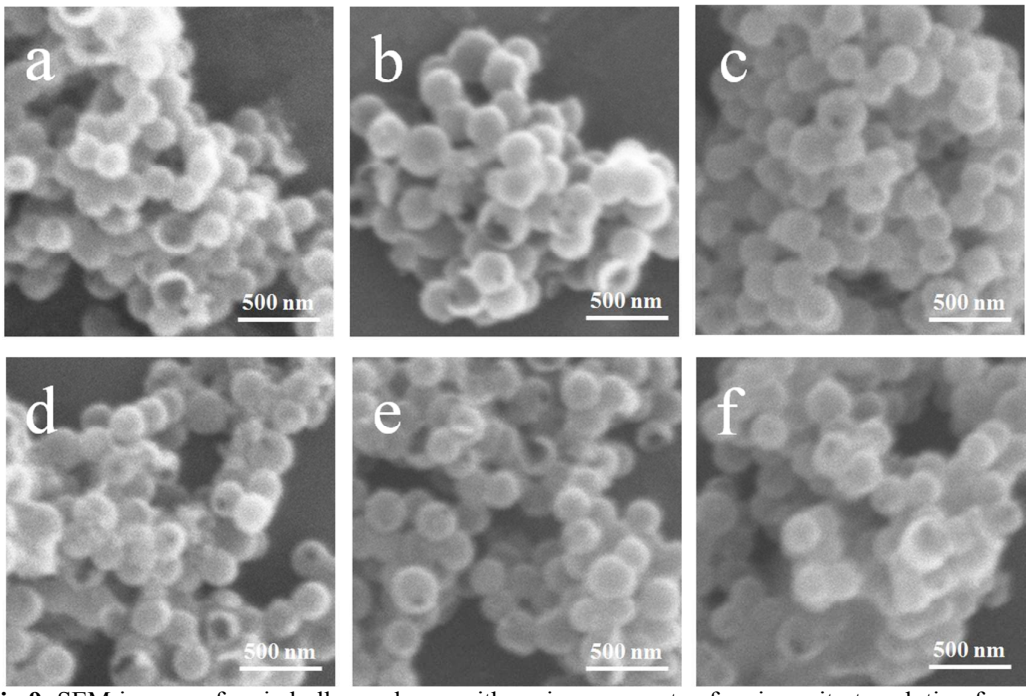

Fig 9. SEM images of ceria hollow spheres with various amounts of cerium nitrate solution from 14 mL to 24 mL

Effect of temperature of calcination

To elucidate the change and evolution of phase compositions, crystallization of composite spheres after calcination at different temperatures was checked by XRD. Fig. 10 shows the XRD patterns of the composite spheres annealed at 400, 500, 600, 700 and 800 ^{o}C for 2 h. All the diffraction peaks at 2 θ values at different calcination temperature have the same values accordingly indicating that CeO_2 has cubic crystalline structure. However, the peaks intensity increase with calcination temperature increase, indicating crystallinity of CeO_2 shells increase with calcination temperature increase. Fig. 11 shows a comparison of the morphologies of the products obtained at calcination temperatures of 400, 600, 700 and 800 ^{o}C. The products remain spherical after calcination until at 700 ^{o}C (Fig 11 a-c). However, after calcination at 800 ^{o}C, hollow spheres aggregated. This morphological evolution is explained with the atomic migration at high temperature. With microcosmic atomic migration, the crystal trends to grow in the direction of the plane, which has the highest surface energy. During the calcinations of CeO_2 hollow spheres, the composed particles grow closer and closer together, accumulating to aggregation-like morphology.

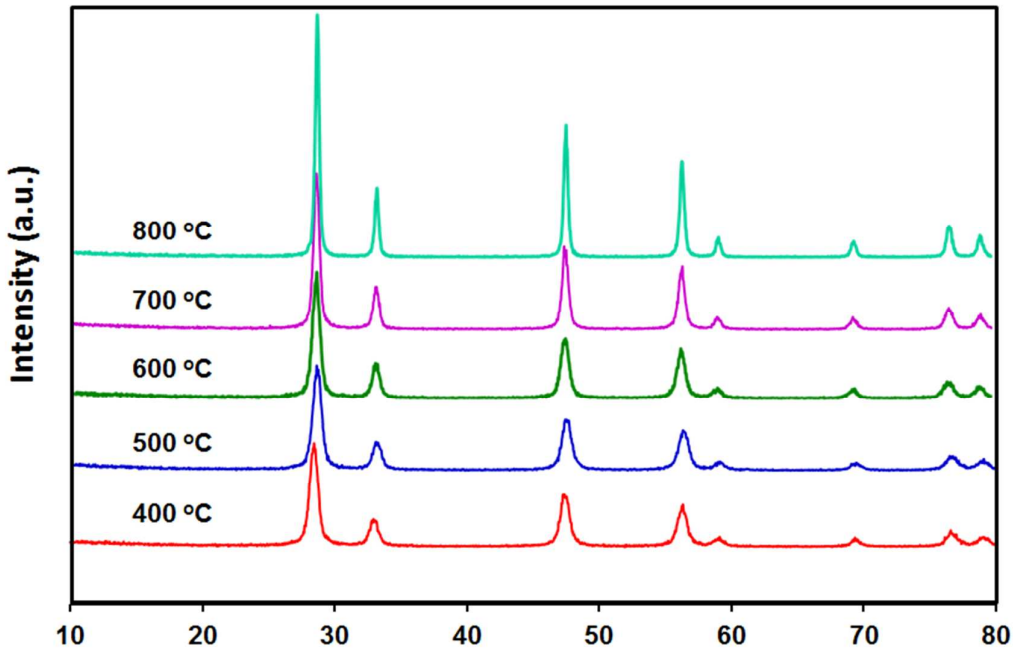

Fig. 10 XRD patterns of the composite spheres calcinated at 400, 500, 600, 700 and 800 ^{o}C for 2 h

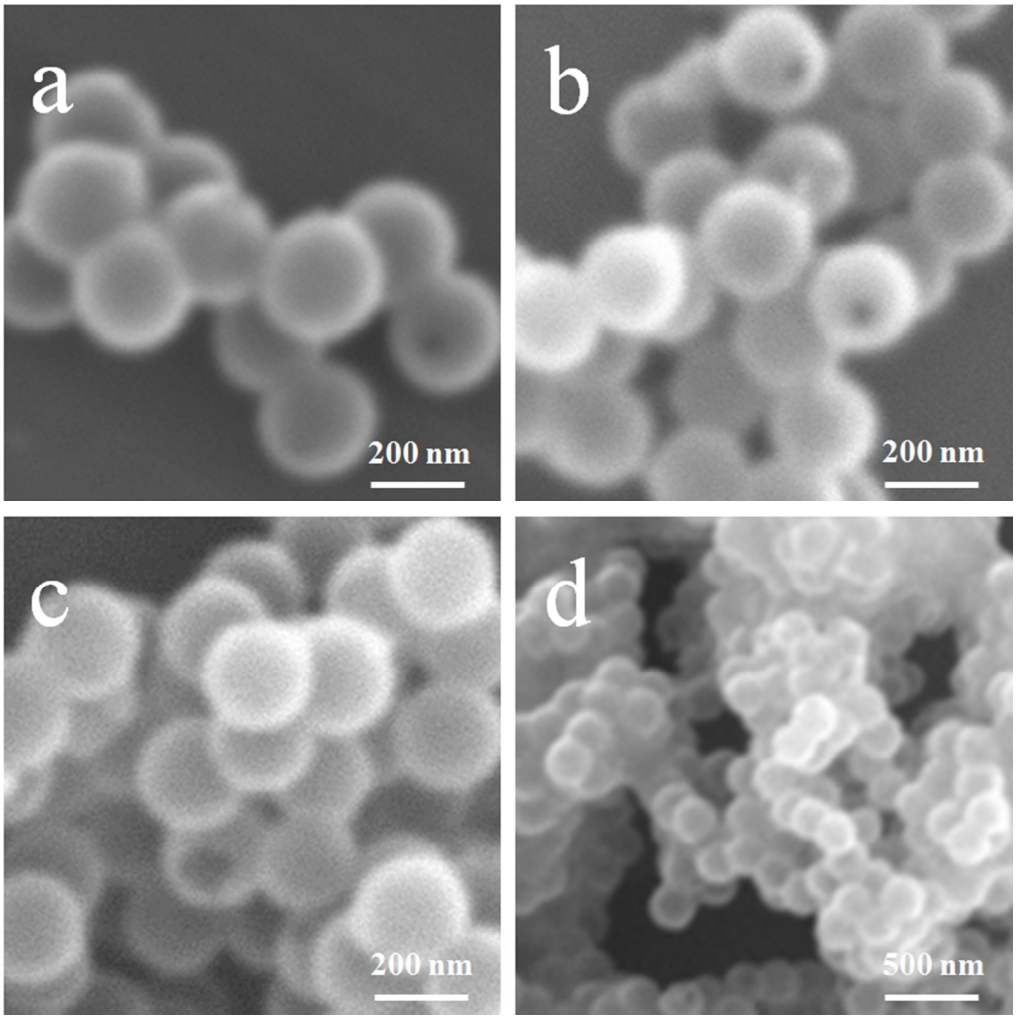

Fig. 11 SEM images of ceria hollow sphere under different temperature

Formation mechanism of ceria hollow spheres

Based on above discussion, the mechanism of ceria hollow sphere formation is described in Fig. 12. First, monodisperse PSAA spheres are synthesized which are negatively charged by –COO- groups on the surface. Second, when ceria precursor is mixed with PSAA spheres, Ce^{3+} ions are absorbed on the surface of PSAA via electrostatic interaction. Third, sol-gel suspension forms simultaneously as ammonia solution is added gradually. As a result, absorbed Ce^{3+} ions serve as nucleation sites and $Ce(OH)_3$ particles are coated on the surface of PSAA beads. With gradual pH increase, seeds of $Ce(OH)_3$ particles keep on growing and form a smooth coat on PSAA spheres. Finally, ceria hollow spheres are fabricated after PSAA removal with calcination and synchronously amorphous $Ce(OH)_3$ particles transfer to crystalline ceria structure which show excellent photocatalytic activity. When ceria hollow spheres are applied in photocatalysis, morphology of hollow spheres improves the photocatalytic activity by light capture with lights transmission and their reflection inside hollow spheres.

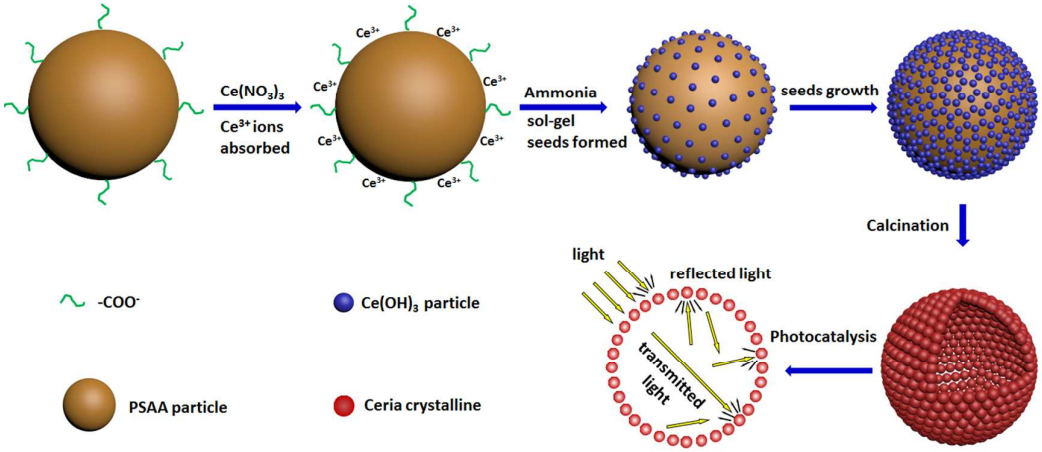

Fig. 12 Schematic illustration of the synthesis of ceria hollow spheres and their photocatalysis enhancement

Photocatalytic activity of ceria hollow spheres

Fig. 13a shows UV-visible adsorption spectra of ceria hollow spheres and commercial ceria nanoparticles. Ceria hollow spheres exhibit increased absorption in both UV and visible light region while nanoparticles do limited absorption. This indicates that ceria hollow spheres exhibit higher activity in visible light region. The reason is explained by larger surface area and hollow spheres morphology. As shown in BET test, as-obtained ceria hollow spheres have surface area of 60.6 m^2 g^{-1} while nanopatiles do only 12.95 m^2 g^{-1}. When light radiates on hollow spheres, they not only reflect on surface as normal particle morphology, but also capture more irradiation energy with transmitted lights and their further reflection inside hollow sphere as shown in Fig. 12. Since ceria is direct semiconductor, the E_g value can be calculated as the equation: $(\alpha h\nu)^2=A(h\nu-Eg)$, where α is the absorption coefficient, $h\nu$ is the light energy, A is a constant, E_g is the band gap energy. The plot of $(\alpha h\nu)^2$ versus $h\nu$, is shown in Fig. 13b. The E_g values of both the as-synthesized ceria hollow spheres and nanoparticles are shown to be approximately 3.2 eV, indicating that the E_g value does not change despite huge morphological change. Photodegradation experiment were carried out under visible light using RhB as probe reaction in aqueous suspension. Before irradiation, the suspensions were kept in the dark for 30 min to establish adsorption-desorption equilibrium between the photocatalyst and RhB. In Fig 13e RhB absorption of CeO_2 particles and CeO_2 hollow spheres within 30 min are approximately 7% and 11%, respectively. More RhB absorption on CeO_2 hollow spheres is attributed to larger surface area and pore volume of hollow spheres. Fig. 13e also shows that as-obtained ceria hollow spheres exhibit strong photocatalytic activity of RhB degradation under visible light. After 180 min, there was only 7% RhB remained with ceria hollow spheres while under the same scenario, there was 65.8% RhB remained with commercial nanoparticles. The blank was conducted simultaneously without any catalysts. After 180 min, only 2.4% RhB was degraded. Fig. 13c exhibits adsorption spectra change of RhB photodegradation with ceria hollow spheres. The curves have the same main absorption peak (λ=554 nm) and no new absorption bands are found, indicating complete photodegradation of RhB. The color changes are shown by photo images in Fig. 13d. As shown in Fig. 13f, the relationship between $\ln(C_0/C)$ and irradiation time of the degradation by ceria hollow spheres is not linear, where C_0 and C are the concentration before and after irradiation, respectively. This indicates that the photocatalytic degradations performed using ceria hollow spheres do not follow pseudo-first-order reaction kinetics, which differs from the degradation with P25. In particular, such photodegradation with as-obtained ceria hollow spheres exhibited auto-accelerated effect. It is possible that lanthanides may undergo photodegradation through a different mechanism than common n-type semiconductors[36, 37]. Under light irradiation, the active sites of ceria immobilize dye molecules and the photoinduced electrons and holes on the surfaces attack the dye molecules directly. The acidic intermediates produced from the decomposed dye molecules were found to produce a more acidic environment during the process of photodegradation, allowing ceria hollow spheres to band and degrade more dye molecules. The more active sites on the exposed crystallographic planes during the process of degradation, the

more dyes are bound. The scattering and reflecting of incident light by the hollow-sphere structures increase the light intensity and thus promote the photocatalytic reactions. Eventually, in later stages, ceria hollow spheres exhibit stronger photocatalytic performance. Therefore, it is concluded that as-obtained ceria hollow spheres have excellent photocatalytic activity under visible light.

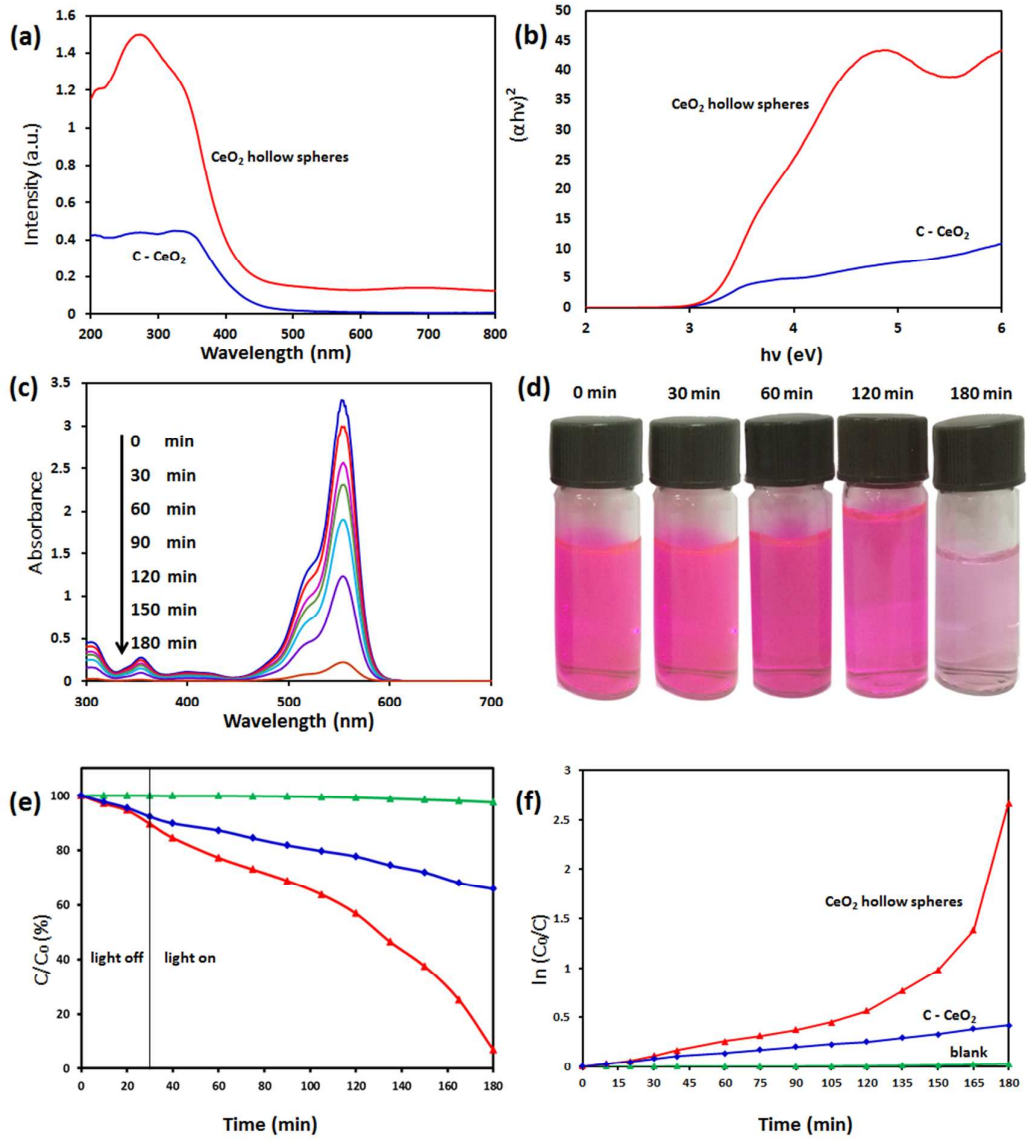

Fig.13 (a) UV-visible adsorption spectra of as-obtained ceria hollow spheres and commercial ceria nanoparticles. (b) The plots of $(\alpha h\nu)^2$ versus hν of as-obtained ceria hollow spheres and commercial ceria nanoparticles. (c) UV-visible absorption spectra in the process of photodegradation of RhB. (d) Photo images of RhB in the adsorption and photodegradation. (e) Degradation efficiency curves. (f) Relationship between irradiation time and ln (C_0/C) of the photocatalytic degradation data shown in panel (e).

Conclusion

In summary, a general and green approach to synthesize monodisperse ceria hollow spheres with tunable shell structure is developed, in which monodisperse negatively charged PSAA spheres are first prepared, and then ceria precursor is coated on PSAA spheres by sol-gel method. During calcination of PSAA removal, ceria precursor synchronously transfer to crystalline structure. The as-obtained ceria hollow spheres exhibit enhanced photocatalytic activity under visible light. Based on this technique, other inorganic hollow spheres with various shell compositions could

also be prepared with scale-up fabrication under aqueous phase.

Reference

1. J. Kaspar, P. Fornasiero, M. Graziani, *Catal. Today*, 1999, 50, 285.
2. C. Sun, R. Hui, J. Roller, *Solid State Electrochem.*, 2010, 14, 1125.
3. R. Juarez, S. F. Parker, P. Concepcion, A. Corma, H. Garcia., *Chem. Sci.*, 2010, 1, 731.
4. P. Jasinski, T. Suzuki, H. U. Anderson, *Sens. Actuators, B,* 2003, 95, 73.
5. Z. Zhang, W. Liu, J. Zhu, Z. Song. *Appl. Surf. Sci.*, 2010, 257, 1750.
6. T. Morimoto, H. Tomonaga and A. Mitani, *Thin Solid Films*, 1999, 351, 61.
7. Y. Jin, N. Li, H. Liu, X. Hua, Q. Zhang, M. Chen, F. Teng, *Dalton Trans.*, 2014, 43, 12860.
8. Z. Tang, Y. Zhang, Y. Xu, *RSC Adv.,* 2011, 1, 1772.
9. A. Macedo, S. Fernandes, A. Valente, R. Ferreira, L. Carlos, J. Rocha, *Molecules,* 2010, 15, 747.
10. J. Chen, S. Patil, S. Seal, J. McGinnis, *Nat. Nanotechnol.,* 2006, 1, 142.
11. J. Holgado, R. Alvarez, G. Munuera. *Appl. Surf. Sci.*, 2000, 161, 301.
12. C. Sun, H. Li, L. Chen, *Energ. Environ. Sci.*, 2012, 5, 8475.
13. C. Sun, H. Li, Z. Wang, L. Chen, X. Huang. *Chem. Lett.,* 2004, 662.
14. K. Zhou, X. Wang, X. Sun, Q. Peng, Y. Li, *J. Catal.*, 2005, 229, 206.
15. W. Han, L. Wu, Y. Zhu, *J. Am. Chem. Soc.*, 2005, 127, 12814.
16. S. Yang, L. Gao. *J. Am. Chem. Soc.*, 2006, 128, 9330.
17. T. Yu, B. Lim, Y. Xia. *Angew. Chem.*, 2010, 122, 4586.
18. I. Yamaguchi, M. Watanabe, T. Shinagawa, M. Chigane, M. Inaba, A. Tasaka, M. Izaki. *ACS Appl. Mater. Inter.*, 2009, 1, 1070.
19. Y. Wei, J. Liu, Z. Zhao, A. Duan, G. Jiang, C. Xu, J. Gao, H. He, X. Wang, *Energ. Environ. Sci.*, 2011, 4, 2959.
20. A. Mann, Z. Wu, F. Calaza, S. Overbury. *ACS Catal.*, 2014, 4, 2437.
21. R. Caruso, A. Susha, F. Caruso. *Chem. Mater.*, 2001, 13, 400.
22. J. Hu, M. Chen, X. Fang, L. Wu. *Chem. Soc. Rev.*, 2011, 40, 5472.
23. J. Zhang, *J. Phys. Chem. Lett.*, 2010, 1, 686.
24. D. Shchukin, R. Caruso. *Chem. Mater.*, 2004, 16, 2287.
25. Z. Yang, D. Han, D. Ma, H. Liang, L. Liu, Y. Yang, *Cryst. Growth Des.,* 2010, 10, 291.
26. Z. Yang, J. Wei, H. Yang, L. Liu, H. Liang, Y. Yang, *Eur. J. Inorg. Chem.*, 2010, 3354.
27. X. Liu, H. Yang, L. Han, W. Liu, C. Zhang, X. Zhang, S. Wang, Y. Yang, *CrystEngComm*, 2013, 15, 7769.
28. N. Strandwitz, G. Stucky. *Chem. Mater.*, 2009, 21, 4577.
29. Z. Guo, F. Jian, F. Du. *Scripta Mater.*, 2009, 61, 48.
30. J. Qian, Z. Chen, C. Liu, X. Lu, F. Wang, M. Wang, *Mat. Sci. Semicon. Proc.,* 2014, 25,27.
31. F. Chen, W. Wang, Z. Chen, T. Wang. *J. Rare Earth.*, 2012, 30,350.
32. R. Gao, M. Chen, W. Li, S. Zhou, L. Wu, *J. Mater. Chem. A,* 2013, 1, 2183.
33. Z. Yang, T. Woo, M. Baudin, K. Hermansson, *J. Chem. Phys.*, 2004, 120, 7741.
34. Z. Deng, M. Chen, S. Zhou, B. You, L. Wu. *Langmuir*, 2006, 22, 6403.
35. M. Chen, L. Wu, S. Zhou, B. You. *Adv. Mater.*, 2006, 18, 801.
36. Y. Zhao, C. Eley, J. Hu, J.S. Foord, L. Ye, H. He, S.C.E. Tsang, *Angew. Chem. Int. Edit.*, 2012, 51, 3846.
37. W. Li, R. Gao, M. Chen, S. Zhou, L. Wu. *J. Colloid Interf. Sci.*, 2013, 411, 220.

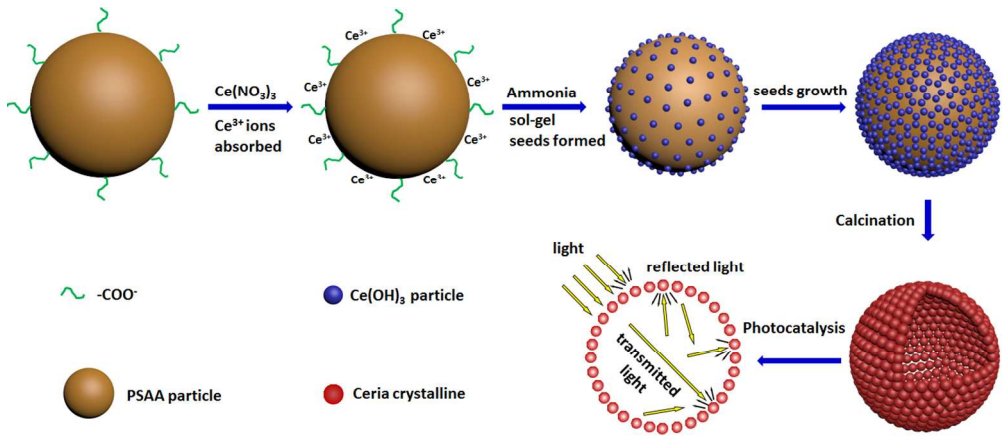

373x161mm (96 x 96 DPI)